Protein Science (2000), *9*:1194–1202. Cambridge University Press. Printed in the USA.

Unfolding and refolding of cytochrome *c* driven by the interaction with lipid micelles

NARINDER SANGHERA AND TERESA J.T. PINHEIRO

Department of Biological Sciences, University of Warwick, Gibbet Hill Road, Coventry CV4 7AL, United Kingdom

(RECEIVED December 13, 1999; FINAL REVISION March 20, 2000; ACCEPTED April 3, 2000)

Abstract

Binding of native cyt *c* to L-PG micelles leads to a partially unfolded conformation of cyt *c*. This micelle-bound state has no stable tertiary structure, but remains as α-helical as native cyt *c* in solution. In contrast, binding of the acid-unfolded cyt *c* to L-PG micelles induces folding of the polypeptide, resulting in a similar helical state to that originated from the binding of native cyt *c* to L-PG micelles. Far-ultraviolet (UV) circular dichroism (CD) spectra showed that this common micelle-associated helical state (H_L) has a native-like α-helix content, but is highly expanded without a tightly packed hydrophobic core, as revealed by tryptophan fluorescence, near-UV, and Soret CD spectroscopy. The kinetics of the interaction of native and acid-unfolded cyt *c* was investigated by stopped-flow tryptophan fluorescence. Formation of H_L from the native state requires the disruption of the tightly packed hydrophobic core in the native protein. This micelle-induced unfolding of cyt *c* occurs at a rate $\sim$0.1 s^{-1}, which is remarkably faster in the lipid environment compared with the expected rate of unfolding in solution. Refolding of acid-unfolded cyt *c* with L-PG micelles involves an early highly helical collapsed state formed during the burst phase ($<$3 ms), and the observed main kinetic event reports on the opening of this early compact intermediate prior to insertion into the lipid micelle.

Keywords: collapsed state; cytochrome *c*; folding intermediates; folding in lipid membranes; folding kinetics; membrane insertion; unfolding in lipid membranes

Cyt *c* functions in electron transfer on the surface of the inner mitochondrial membrane. The potential involvement of a membrane-bound form of cyt *c* in electron transfer has been unclear (Vik et al., 1981; Speck et al., 1983; Gupte & Hackenbrock, 1988; Hildebrandt et al., 1990) until the recent work by Cortese et al. (1998). This work showed that under physiological conditions, cyt *c* is found to be in equilibrium between the soluble state and conformations bound to the inner mitochondrial membrane. These membrane-bound species have a destabilized structure compared with the native protein, but retain variable degrees of electron transfer activities, depending on their binding state to the inner mitochondrial membrane. This suggests that membrane-bound forms of cyt *c* could regulate the activity of electron transfer in vivo.

Cyt *c* has also been found to play a role in programmed cell death (apoptosis), in which the release of cyt *c* from the mitochondrion is required for caspase activation (Liu et al., 1996; Hu et al., 1999). A recent study by Jemmerson et al. (1999) has shown that a membrane-bound form of cyt *c* has apoptotic activity, suggesting that membrane-associated cyt *c* might be the relevant factor in caspase activation. Thus, with the increasing evidence for physiological roles of membrane-bound forms of cyt *c*, both in electron transfer (Cortese et al., 1998) and in apoptosis (Jemmerson et al., 1999), it is pertinent to investigate the structural and dynamic properties of membrane-bound forms of cyt *c*.

It has been known that binding of cyt *c* to negatively charged lipid membranes induces an extensive disruption of the native compact structure of the protein (Muga et al., 1991; Spooner & Watts, 1991; de Jongh et al., 1992; Pinheiro & Watts, 1994; Pinheiro et al., 1997). This membrane-bound state lacks many features of its native tertiary structure but remains highly helical. Far-UV CD spectra showed that this partially unfolded state bound to lipid membranes has an α-helix content similar to that of the native protein in solution. Tryptophan fluorescence and heme absorbance kinetics revealed that the disruption of the tightly packed native structure of cyt *c* is remarkably accelerated on the membrane interface compared with the expected rate of unfolding in solution (Pinheiro et al., 1997).

In contrast, binding of the unstructured precursor protein, apocyt *c*, to lipid membranes induces folding of the polypeptide that can generate a partially folded conformation with an α-helix content that resembles that of native cyt *c* (Jordi et al., 1989; de Jongh & de Kruijff, 1990; Rankin et al., 1998). The level of lipid-induced secondary structure depends on the lipid system, and this folding process is driven by both electrostatic and hydrophobic lipid-

Reprint requests to: Dr. Teresa J.T. Pinheiro, Department of Biological Sciences, University of Warwick, Gibbet Hill Road, Coventry CV4 7AL, United Kingdom; e-mail: tpinheiro@bio.warwick.ac.uk.

Abbreviations: CD, circular dichroism; cyt *c*, cytochrome *c*; DOPS, dioleoylphosphatidylserine; GuHCl, guanidine hydrochloride; L-PG, lysophosphatidylglycerol (1-myristoyl-2-hydroxy-*sn*-glycero-3-[phospho-*rac*-(1-glycerol)]); UV, ultraviolet.

protein interactions (Rankin et al., 1998). Kinetic measurements revealed that folding of apocyt *c* induced by negatively charged lipid micelles occurs via a collapsed intermediate state prior to insertion into the lipid micelle (Rankin et al., 1999), while folding induced by zwitterionic lipid micelles involves a more distended intermediate on the micelle surface (Bryson et al., 1999).

Protein folding and unfolding on the surface of membranes are essential biological processes in protein translocation across membranes, protein assembly, and function. For example, large structural rearrangements are involved in the insertion of bacterial toxins in target cell membranes (van der Goot et al., 1991; Vécsey-Semjén et al., 1997; Zakharov et al., 1998) and required for the transfer of various nonpolar ligands, such as retinol and fatty acids, from their carrier proteins to a target cell surface (Bychkova & Ptitsyn, 1993). In contrast with native stably-folded proteins, which may become destabilized by the interaction with membranes, many peptides and proteins with little or no structure in solution can acquire secondary structure upon binding to lipid membranes. Among those are small toxins (Thieudière et al., 1991; Shai, 1994), antimicrobial peptides (Maloy & Kari, 1995), signal sequences (Gierasch, 1989), and apocytochrome *c* (Jordi et al., 1989; de Jongh & de Kruijff, 1990; Rankin et al., 1998).

Cyt *c* and its heme-free precursor (apocyt *c*) are a unique pair with respect to their interaction with lipid membranes. While cyt *c* partially unfolds upon binding to lipid membranes, apocyt *c*, which is a random coil in aqueous solution, acquires an α-helical structure upon interaction with lipid membranes. The mechanism by which a tightly folded water-soluble protein becomes associated with a membrane is not completely understood, nor is the folding of an unfolded polypeptide in lipid membranes. It is apparent that the association with the membrane triggers the protein structural changes, but there is very little information available on the nature of the intermediate states involved in folding or unfolding events in lipid membranes. It has been postulated that the membrane-bound helical conformations of both cyt *c* and apocyt *c* might represent a common folded state (de Jongh et al., 1992; Pinheiro, 1994). However, a direct comparison of the membrane-induced unfolding and refolding of cyt *c* is missing, as there are no studies available on refolding of cyt *c* in lipid membranes.

In the current study, we have characterized the structural properties of both native and acid-unfolded cyt *c* upon interaction with negatively charged lipid micelles of L-PG. Binding of native cyt *c* to L-PG micelles leads to a partially unfolded conformation of cyt *c*. This micelle-bound state has no stable tertiary structure, but remains as α-helical as native cyt *c* in solution. In contrast, binding of the acid-unfolded cyt *c* to L-PG micelles induces the folding of the polypeptide and results in a similar helical state to that originated from the binding of native cyt *c* to L-PG micelles. The kinetics of the interaction of native and acid-unfolded cyt *c* was investigated by stopped-flow tryptophan fluorescence and their respective unfolding and refolding mechanisms are proposed. The possible biological roles of membrane-associated partially folded states of cyt *c* in electron transfer and apoptosis are discussed.

Results

Soret absorbance

Absorbance measurements in the Soret region (350–490 nm) report on the spin state of the heme iron. Under native conditions, the heme iron is in a low-spin state with two axial ligands provided from His18 and Met80. A Soret band with a maximum intensity at 410 nm (λ_{max}) is typical of the native state of cyt *c*, indicative of the presence of both axial ligands. In contrast, during acid unfolding the heme iron is converted to a high-spin state, probably lacking both Met80 and His18 ligation (Babul & Stellwagen, 1972), which results in a blue shift of the Soret band of about 15 nm. Binding of acid-unfolded cyt *c* to L-PG micelles results in a shift of the Soret λ_{max} from 394 to 403 nm, and binding of native cyt *c* is accompanied by a shift from 410 to 407 nm (Fig. 1). The blue shift for the Soret band observed upon binding of native cyt *c* to L-PG micelles is consistent with disruption of Met80 ligation to the heme iron, as observed for the binding of cyt *c* to lipid membranes (Pinheiro et al., 1997). Binding of acid-unfolded cyt *c* to L-PG micelles results in a spectrum that approaches that of cyt *c* bound to L-PG micelles originated from the native state. However, the observed differences in λ_{max} may arise from nonnative histidine ligation to the heme iron in unfolded cyt *c* (Colón et al., 1997).

Equilibrium fluorescence

The fluorescence emission of the single tryptophan at position 59 (Trp59) in the polypeptide chain of cyt *c* was used to monitor conformational changes in the protein upon interaction with L-PG micelles. In the native fold of cyt *c*, Trp59 is located near the heme group (center-to-center distance Trp59-heme is 9.5 Å; Bushnell et al., 1990), which results in an efficient quenching of Trp59 fluorescence (Fig. 2). Under strong denaturing conditions (4.2 M GuHCl, or pH 2 and low ionic strength), the fluorescence spectrum has an emission maximum near 350 nm with an intensity ~60% of that of a corresponding aqueous solution of free tryptophan. These changes are consistent with a highly expanded conformation of the polypeptide chain (Tsong, 1974). Binding of acid-unfolded cyt *c* to

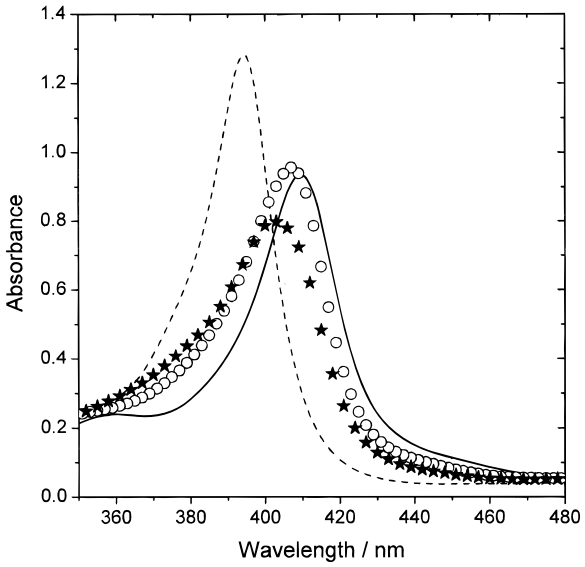

Fig. 1. Absorbance spectra of the Soret region of acid-unfolded cyt *c* (dashed line) in aqueous solution and after binding to L-PG micelles (stars), and native cyt *c* in aqueous solution (solid line) and after binding to L-PG micelles (circles). Protein concentration was 10 μM, and lipid concentration was 2 mM. Spectra were recorded at room temperature (~22 °C).

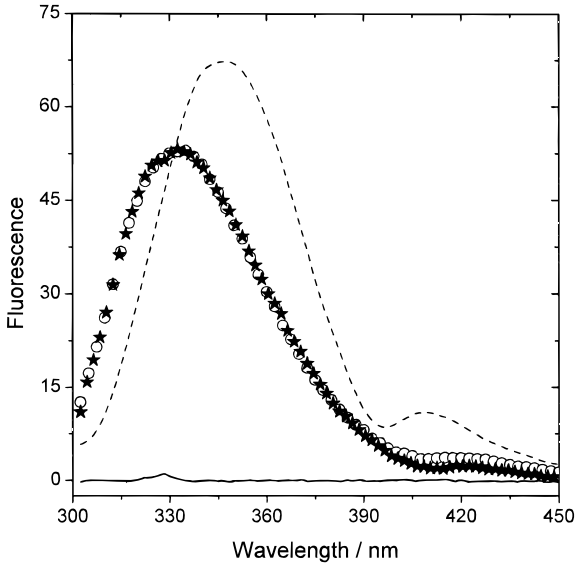

Fig. 2. Fluorescence emission spectra of native cyt *c* in aqueous solution (solid line) and after binding to L-PG micelles (circles), and acid-unfolded cyt *c* (dashed line) and after binding to L-PG micelles (stars). Protein concentration was 10 μM, and L-PG concentration was 2 mM. The spectra were recorded at room temperature (~22 °C) with excitation at 295 nm.

L-PG micelles is accompanied by a blue shift of about 15 nm relative to the emission maximum of acid-unfolded cyt *c*, and a similar spectrum is also obtained upon binding of native cyt *c* to L-PG micelles (Fig. 2).

Circular dichroism

Circular dichroism was used to probe structural changes in cyt *c* upon the interaction with L-PG micelles. The far-UV CD spectrum of cyt *c* in aqueous solution (Fig. 3A) is typical of proteins containing mainly α-helical structure. In contrast, acid-unfolded cyt *c* exhibits a spectrum with a strong negative band near 200 nm, which is characteristic of a disordered polypeptide chain. Binding of native and acid-unfolded cyt *c* to L-PG micelles results in similar spectra, which show no significant changes in the far-UV CD band at 222 nm when compared with the spectrum of native cyt *c* in solution (Fig. 3A). This suggests that the micelle-bound state obtained from acid-unfolded or native protein both have an α-helix content that resembles that of the native cyt *c* in solution. The changes around 190 and 208 may arise from spectral contributions of other secondary structural components, or may be due to the presence of optically active heme transitions, other than those associated with the amide transitions of the polypeptide chain (Myer, 1968).

The near-UV CD region (250–330 nm) provides information on the packing of aromatic side chains in the protein. The near-UV CD spectrum of native cyt *c* in aqueous solution displays two distinct minima at 282 and 288 nm, which have been assigned to the tertiary structural packing of Trp59 (Davies et al., 1993). Binding of native cyt *c* to L-PG micelles results in the disappearance of these two bands (Fig. 3B), which is consistent with a disruption of the tight packing of core residues in cyt *c* upon interaction with the lipid micelles. The spectrum obtained with acid-unfolded cyt *c* after binding to lipid micelles also did not show the Trp bands.

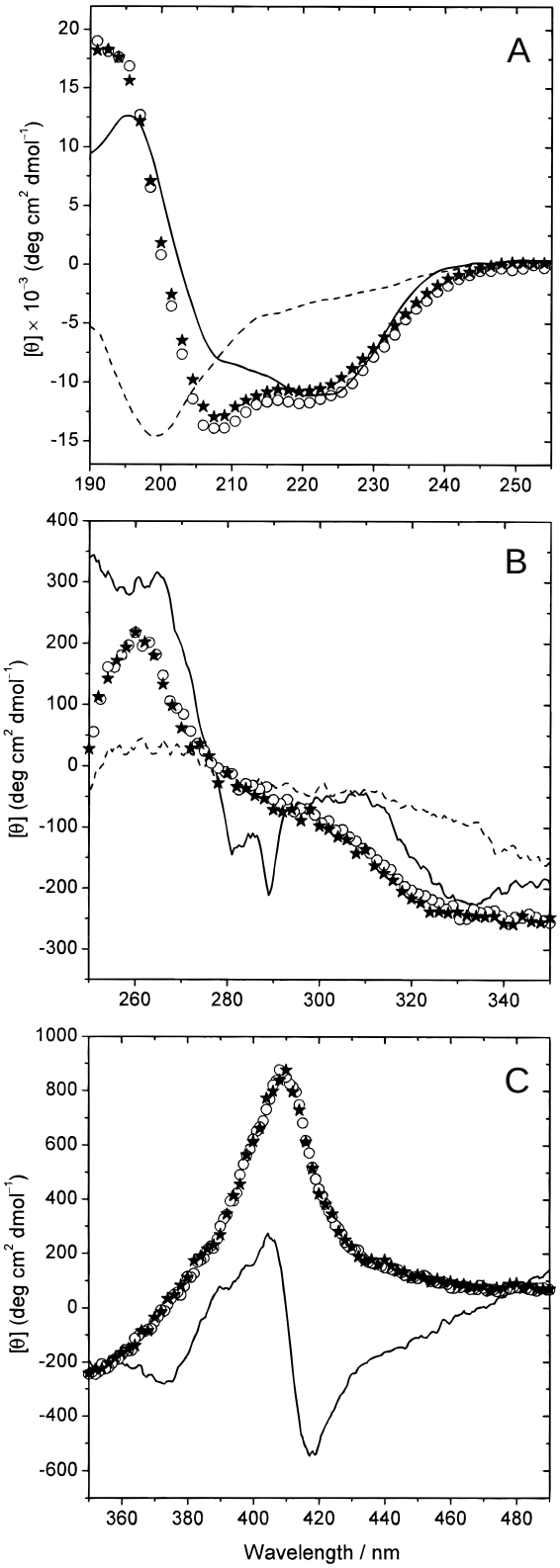

Fig. 3. (**A**) Far-UV, (**B**) near-UV, and (**C**) Soret regions of CD spectra of native cyt *c* in aqueous solution (solid line) and after binding to L-PG micelles (circles), and acid-unfolded cyt *c* (dashed line) and after binding to L-PG micelles (stars). Protein concentrations were 10 μM (far-UV) and 20 μM (near-UV and soret), and L-PG concentration was 2 mM. All spectra were acquired at 20 °C, with a resolution of 0.5 nm/min, but for clarity symbols are only shown every 1.5 or 2 nm.

The CD spectrum in the Soret region (350–490 nm) can provide further insight into the integrity of the heme crevice (Myer, 1968). The optical activity in this region is generated through the coupling of heme π-π* electric dipole transition moments with those of nearby aromatic residues in the protein. The spectrum for cyt *c* in its native conformation exhibits a strong negative band at about 418 nm due to the Soret–Cotton effect (Fig. 3C), primarily a result of heme-polypeptide interactions. After binding of native cyt *c* to L-PG micelles, the Soret CD spectrum is converted to a single positive band with a maximum near 408 nm, identical to that obtained upon binding acid-unfolded cyt *c* to L-PG micelles. This type of spectrum is also obtained for urea- or acid-denatured cyt *c* (Myer, 1968) and has also been observed for cyt *c* bound to DOPS vesicles (Pinheiro et al., 1997). The Soret spectral changes indicate that the coupling between the heme π-π* transitions and those of the aromatic residues nearby have been disrupted upon binding of native cyt *c* to lipid micelles and that no such interactions are present in the helical state formed from acid-unfolded cyt *c*.

Kinetics of unfolding and refolding of cyt c upon binding to L-PG micelles

The interaction of native cyt *c* with L-PG micelles induces a partial unfolding of the tight native structure of cyt *c*, whereas binding of acid-unfolded cyt *c* to L-PG micelles results in folding into an α-helical state. Tryptophan fluorescence changes were used to monitor the kinetics of the interaction of both acid-unfolded and native cyt *c* with L-PG micelles in stopped-flow measurements. Typical kinetic traces for the refolding of acid-unfolded cyt *c* and unfolding of native cyt *c* upon interaction with L-PG micelles are shown in Figure 4.

The interaction of acid-unfolded cyt *c* (U) with L-PG micelles (micelle-induced refolding) comprises four kinetic events. There is an initial decrease in fluorescence during the dead time of the instrument ~2.7 ms (burst phase). The amplitude of this burst phase (the drop in signal relative to the initial fluorescence level of U) varied from 50–65% of the fluorescence of U, depending on protein and lipid concentration. This is followed by an increase in fluorescence, which is described by three main kinetic phases (Table 1). (1) A fast phase (k_1) accounting for 10–21% of the total observed fluorescence change occurs over 100–400 ms; (2) an intermediate phase (k_2) associated with the largest increase in fluorescence (62–80%) occurring over 1–3 s; and (3) a slow phase (k_3) in which 8–17% of the total fluorescence increase is observed over a time range larger than 30 s.

The interaction of native cyt *c* (N) with lipid micelles (micelle-induced unfolding) shows no burst phase (Fig. 4) and the increase in fluorescence associated with the partial unfolding and insertion into the lipid micelle is also described by three main kinetic phases (Table 2). (1) Fast phase (k_1) carrying a small fraction of the total observed fluorescence change (<10%) occurs over a time scale from 200 ms to 1.2 s. (2) An intermediate phase (k_2) occurring in <10 s is associated with the largest change in fluorescence (76–97%). (3) A slow phase (k_3) in which up to 19% of the fluorescence increase occurs over a time range larger than 10 s. This phase becomes negligible for high lipid-to-protein ratios.

The observed kinetics of micelle-induced refolding and unfolding of cyt *c* are overall similar (Tables 1, 2), but a close inspection of their kinetic parameters reveals some significant differences. The fast phase (k_1) for the micelle-induced refolding reaction occurs in <0.5 s, whereas unfolding extends from 200 ms to 1.2 s for equivalent lipid and protein concentrations. The relative amplitude associated with this phase (a_1) increases from 12 to 21% with increasing protein concentration for refolding (Table 1), but a_1 represents only ~5% of the total fluorescence increase and is independent of protein concentration for unfolding. The intermediate phase (k_2), which for both refolding and unfolding accounts for the largest change in fluorescence, is faster for refolding than for unfolding (Tables 1, 2).

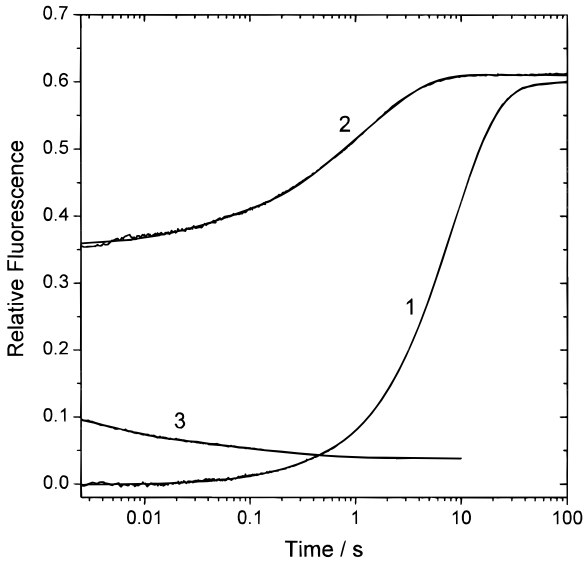

Fig. 4. Representative unfolding and refolding kinetic traces of cyt *c* upon interaction with L-PG micelles at 20 °C. Trp59 fluorescence emission (excited at 295 nm and detected above 310 nm) was measured in stopped-flow measurements, following rapid mixing of protein with L-PG micelles (dead time ~2.7 ms). Lipid backgrounds were subtracted, and all traces were normalized relative to the fluorescence level of acid-unfolded protein. The fluorescence changes are plotted on a logarithmic timescale for the interaction of native (1) and acid-unfolded (2) cyt *c* with L-PG micelles. Lipid concentration was 2 mM, and protein concentration was 10 μM. For comparison the refolding of cyt *c* in the absence of lipid from the acid-unfolded state in 10 mM HCl, pH 2.0 into 10 mM phosphate buffer, pH 7.0 is also shown (3). Lines represent double or triple exponential fits to the experimental data.

Discussion

Binding of native and acid-unfolded cyt c to L-PG micelles leads to a common micelle-bound helical state as determined by CD and fluorescence

The fluorescence of the single tryptophan (Trp59) in the compact native structure of cyt *c* is efficiently quenched due to its close proximity to the heme group (Fig. 2). Upon unfolding of cyt *c*, the expanding Trp59-heme distance leads to a large increase in fluorescence (up to ~60% of that of free tryptophan) indicative of an expanded conformation with an average Trp59-heme distance >35 Å (Tsong, 1974; Chan et al., 1997). Binding of native or acid-unfolded cyt *c* to L-PG micelles resulted in equivalent spectra, with a λ_{max} blue-shifted by ~15 nm relative to the emission maximum of the acid-unfolded state in solution. The fluorescence emission spectra of micelle-bound cyt *c*, originated from either native

Table 1. *Kinetic parameters for the interaction of acid-unfolded cyt c with L-PG micelles at various protein and lipid concentrations*[a]

[L-PG] (mM)	[cyt *c*] (μM)	k_1 (s^{-1})	a_1 (%)[b]	k_2 (s^{-1})	a_2 (%)[b]	k_3 (s^{-1})	a_3 (%)[b]	a_{tot}[c]
8	4	2.6 (3)[c]	12	0.48 (1)	74	0.033 (3)	14	−0.23
8	8	3.3 (1)	10	0.613 (4)	80	0.016 (1)	10	−0.46
8	12	9.8 (2)	17	0.714 (4)	72	0.014 (2)	11	−0.79
8	16	8.6 (2)	19	0.733 (4)	65	0.005 (2)	16	−1.10
8	20	7.6 (1)	21	0.729 (4)	62	0.004 (2)	17	−1.35
2	10	4.6 (1)	16	0.313 (2)	73	0.028 (2)	11	−0.71
5	10	9.7 (2)	16	0.489 (2)	76	0.021 (2)	8	−0.68
10	10	8.92 (2)	16	0.815 (4)	72	0.005 (2)	12	−0.72

[a] Rates and relative amplitudes were measured by stopped-flow fluorescence emission kinetic measurements at 20 °C, as described under Materials and methods.
[b] Percentage of the total amplitude.
[c] Total amplitude ($a_{tot} = a_1 + a_2 + a_3$) in arbitrary (but constant) fluorescence units.
[d] Errors in the least significant digit (one standard deviation) are shown in parentheses.

or acid-unfolded protein, represent ~77% of the fluorescence intensity of the acid-unfolded state (Fig. 2). Binding of the peptide Lys-Trp-Lys to L-PG micelles showed a blue shift of ~14 nm relative to the emission maximum in aqueous solution with no significant changes in the overall fluorescence intensity (data not shown). Thus, the intensity changes of Trp59 fluorescence for cyt *c* in the lipid environment result predominantly from changes in the heme-Trp59 distance associated with unfolding or refolding of cyt *c*. The blue shift for the fluorescence spectra of micelle-bound cyt *c* relative to the λ_{max} of acid-unfolded protein is consistent with the change in the Trp environment from an aqueous solution to the lipid hydrophobic phase. Similar fluorescence changes have been reported for the interaction of cyt *c* with negatively charged lipid vesicles and have been associated with a partial unfolding of cyt *c* (Pinheiro et al., 1997).

Binding of native cyt *c* to L-PG micelles results in a far-UV CD spectrum with no significant changes around the 222 nm band (Fig. 3A), which suggests that the micelle-associated state has an identical α-helix content to that of the native protein. The acid-unfolded state is also converted to an identical helical conformation, which resembles the structure of native cyt *c*. The near-UV and Soret CD spectra of micelle-bound cyt *c*, originated either from native or acid-unfolded protein (Fig. 3B,C), indicate that the resulting helical state associated with L-PG micelles has no compact tertiary structure. Thus, binding of native cyt *c* to L-PG micelles induces no significant change in the α-helix content of cyt *c*, but induces the disruption of the tightly packed hydrophobic core characteristic of native cyt *c*. In contrast, the acid-unfolded protein is folded to a helical state also resembling the α-helical structure of native cyt *c*. This micelle-bound helical state originated from the acid-unfolded protein has also no indication of any stable packing of aromatic side chains. Thus, binding of either native or acid-unfolded cyt *c* to L-PG micelles results in an identical conformation with native-like α-helical content but without any stable tertiary structure. The structural properties of this micelle-associated helical state of cyt *c* are identical to the properties previously described

Table 2. *Kinetic parameters for the interaction of native cyt c with L-PG micelles at various protein and lipid concentrations*[a]

[L-PG] (mM)	[cyt *c*] (μM)	k_1 (s^{-1})	a_1 (%)[b]	k_2 (s^{-1})	a_2 (%)[b]	k_3 (s^{-1})	a_3 (%)[b]	a_{tot}[c]
8	4	0.86 (4)[d]	8	0.110 (2)	92	—[e]	—[e]	−0.82
8	8	1.99 (8)	6	0.116 (1)	94	—[e]	—[e]	−1.45
8	12	3.4 (1)	4	0.136 (1)	80	0.055 (1)	16	−2.20
8	16	3.2 (1)	4	0.133 (1)	79	0.063 (1)	17	−2.85
8	20	4.7 (1)	5	0.138 (1)	76	0.066 (1)	19	−3.52
2	10	5.6 (1)	2	0.124 (1)	93	0.049 (3)	5	−2.13
5	10	4.4 (2)	3	0.121 (1)	97	—[e]	—[e]	−2.19
10	10	1.12 (6)	4	0.112 (1)	97	—[e]	—[e]	−2.23

[a] Rates and relative amplitudes were measured by stopped-flow fluorescence emission kinetic measurements at 20 °C, as described under Materials and methods.
[b] Percentage of the total amplitude.
[c] Total amplitude ($a_{tot} = a_1 + a_2 + a_3$) in arbitrary (but constant) fluorescence units.
[d] Errors in the least significant digit (one standard deviation) are shown in parentheses.
[e] Phase not observed.

for a bilayer-bound state resulting from the binding of native cyt *c* to DOPS vesicles (Pinheiro et al., 1997), as revealed from the absorbance, fluorescence, and CD results. These findings indicate that lysophospholipid micelles serve as good model membranes, resulting in identical structural and folding effects as those observed for cyt *c* with lipid vesicles.

Kinetic mechanism of unfolding and refolding of cyt c induced by L-PG micelles

Fluorescence intensity changes of Trp59 have been used to study the refolding of cyt *c* in aqueous solution (Elöve et al., 1992; Colón et al., 1996; Shastry & Roder, 1998) and the partial unfolding of native cyt *c* induced by the interaction with lipid vesicles (Pinheiro et al., 1997). During refolding of cyt *c*, the fluorescence decays due to Förster energy transfer between Trp59 and the heme group. Conversely, unfolding of cyt *c* is accompanied by a fluorescence increase.

Binding of native cyt *c* to negatively charged micelles of L-PG induced a fluorescence increase during stopped-flow measurements, which is consistent with a partial unfolding of cyt *c*. The Trp59 stopped-flow results (Table 2) showed three main kinetic events for this micelle-induced unfolding process: (1) a fast phase (k_1) with a rate $\sim$4 s^{-1}, and associated with a small fluorescence change (up to 8% of the total observed fluorescence change); (2) an intermediate phase with the largest fluorescence change (up to 97% of the total change) occurring at a rate $\sim$0.1 s^{-1}; and (3) a slow phase with a rate $\sim$0.06 s^{-1}, probably associated with protein–protein interactions or lipid rearrangements around cyt *c*.

The intermediate phase (k_2), associated with the largest amplitude (Table 2), is likely to correspond to the main unfolding structural event. The large increase in fluorescence is consistent with the disruption of the tightly packed hydrophobic core of native cyt *c*, leading to a partially unfolded state with an expanded Trp59-heme distance. This micelle-induced unfolding occurs at a rate $\sim$0.1 s^{-1}, which is much faster than the expected rate of unfolding in solution extrapolated to zero denaturant concentration (5×10^{-6} s^{-1} at pH 7 and 2×10^{-3} s^{-1} at pH 5.0; Colón et al., 1996; Sosnick et al., 1996), indicating that the lipid environment accelerates the structural unfolding of cyt *c*. This effect has also been observed for the lipid-induced unfolding of cyt *c* with negatively charged vesicles of DOPS (Pinheiro et al., 1997).

A possible mechanism of how a negatively charged lipid membrane can promote protein unfolding has been suggested to involve the local acidic environment in the immediate vicinity of the lipid surface relative to the bulk solution (Prats et al., 1986; Pinheiro et al., 1997). It is well known that moderately low pH can lead to partially unfolded states of many proteins (for a review see Ptitsyn, 1995). Interestingly, the rate of the main structural unfolding event of cyt *c* in DOPS vesicles was found to be $\sim$1.5 s^{-1} (Pinheiro et al., 1997), which is faster than the corresponding rate for the unfolding of cyt *c* with L-PG micelles observed in the current study ($k_2 \sim 0.1$ s^{-1}, Table 2). It is expected that in vesicles the tighter packing of the lipid molecules in bilayers should concentrate more H_3O^+ ions near the negative lipid headgroups than around the less tightly packed molecules in a micelle. Thus, the observation of a faster unfolding rate with vesicles than with micelles supports the interpretation that the acceleration of protein unfolding by lipid membranes is in part due to the local low effective pH in the vicinity of the lipid headgroups.

Combining our stopped-flow kinetic results with the well-characterized unfolding mechanism of cyt *c* in solution, we propose a kinetic mechanism for the micelle-induced unfolding of native cyt *c* illustrated by Equation 1:

$$N_w \rightleftharpoons N_s \rightleftharpoons D_i \rightleftharpoons H_L. \quad (1)$$

In this scheme, N_w represents the native state in water; N_s depicts a native-like intermediate associated with the surface of the lipid micelle; D_i denotes a denatured state associated with the membrane interface ready for insertion; and H_L is the final helical micelle-inserted state. Binding of cyt *c* to the micelles ($N_w \rightarrow N_s$) is expected to occur within the dead time of the stopped-flow instrument (<3 ms). This second-order process is probably diffusion-controlled and likely to be accelerated by favorable lipid-protein electrostatic interactions between positive residues on the protein surface and the negatively charged lipid headgroups. Because of the efficient quenching of Trp59 in native-like states and compact intermediates (Elöve et al., 1992, 1994), it is unlikely that the binding event is accompanied by any significant fluorescence changes. This appears to be supported by the absence of a burst phase in the stopped-flow kinetic measurements (Fig. 4).

In our kinetic scheme (Equation 1), the main structural unfolding event ($k_2 \sim 0.1$ s^{-1}) is represented by the kinetic step $N_s \rightarrow D_i$, which is expected to be the rate-limiting step. Once the tightly packed core of cyt *c* is disrupted, hydrophobic residues become exposed and readily available for insertion into the lipid phase.

Rapid mixing of acid-unfolded cyt *c* with L-PG micelles also resulted in fluorescence increase, but only after a large decrease (burst phase) during the dead time of the stopped-flow instrument ($\sim$2.7 ms). A burst phase is always observed in refolding kinetics of cyt *c* in solution in stopped-flow measurements (Roder et al., 1988; Elöve et al., 1992, 1994; Colón et al., 1996), which can only be resolved using continuous-flow methods (Chan et al., 1997; Shastry & Roder, 1998). This rapid decrease in fluorescence relative to the initial unfolded state corresponds to a significant reduction in the average Trp59-heme distance and coincides with a large gain in helical secondary structure (Elöve et al., 1992). These findings are consistent with a collapse of the polypeptide chain at the very early stages of folding leading to a compact intermediate with native-like helical structure. The amplitude of the burst phase for the refolding of cyt *c* in the presence of L-PG micelles corresponds to a drop of 50–65% relative to U_w. The burst phase in the refolding of cyt *c* in solution under similar conditions (Fig. 4) accounts for a drop in fluorescence relative to the acid-unfolded state (U_w) of $\sim$85%. This suggests that binding of acid-unfolded cyt *c* to the lipid micelles occurs in the dead time of the stopped-flow instrument (as seen for the interaction of native cyt *c* with lipid membranes) and appears to be accompanied by a large compaction of the polypeptide chain. This is followed by later phases of increasing fluorescence, which report on further protein structural changes in the lipid micelle, that are associated with an increase of Trp59-heme distance. Thus, our results support a kinetic mechanism for the micelle-induced refolding of cyt *c* represented by Equation 2:

$$U_w \rightleftharpoons C_{w/s} \rightleftharpoons I_i \rightleftharpoons H_L \quad (2)$$

where U_w indicates the unfolded state in water, $C_{w/s}$ represents a collapsed state formed in the aqueous phase or in association with

the micelle surface; I_i denotes an intermediate ready for insertion, equivalent to D_i (Equation 1) formed during unfolding; and H_L is the final helical micelle-inserted state. The large drop in fluorescence during the dead time of the stopped-flow measurements is consistent with the formation of an early collapsed state ($U_w \rightarrow C_{w/s}$). The fact that the amplitude associated with the burst phase during refolding of cyt *c* in the presence of L-PG micelles is smaller than that observed for the refolding of cyt *c* in solution under similar conditions (Fig. 4) suggests that $C_{w/s}$ is likely to represent a mixture of partially collapsed states of protein alone and in association with lipid. The later kinetic phases of increasing fluorescence would then represent the opening of $C_{w/s}$ upon interaction with the lipid micelle leading to less compact states (I_i and H_L). Thus, the second kinetic phase (k_2) with a rate $\sim$0.6 s^{-1}, which is associated with the largest change in fluorescence (62–80%, Table 1), is likely to represent the major structural folding event in association with the lipid micelle. In our scheme (Equation 2), this event is probably associated with the kinetic step $C_{w/s} \rightarrow I_i$. This phase (k_2) resembles the kinetic event reported for the folding of apocyt *c* in the presence of L-PG micelles with a rate $\sim$1 s^{-1}, which has been associated with the unfolding of an early compact intermediate (I_C) into a more extended state prior to insertion into the micelle (Rankin et al., 1999).

Stopped-flow CD measurements for the refolding of apocyt *c* (Bryson et al., 1999) and acid-unfolded cyt *c* (data not shown) with L-PG micelles showed that the recovery of the expected ellipticity signal at 225 nm occurred in $<$2 ms. These results combined with the highly quenched Trp59 fluorescence suggest that both I_C and $C_{w/s}$ are compact intermediates with native-like α-helical structure. The observed kinetic phases of increasing fluorescence are then associated with unfolding of early compact intermediates (both during refolding and unfolding of cyt *c* with L-PG micelles) leading to more extended helical states inserted into the lipid micelle.

Unfolding of cyt *c* in solution requires the Met80 ligand to be displaced before the main structural unfolding process can proceed (Colón et al., 1996, 1997; Sauder et al., 1996). Soret absorbance kinetics shows a single kinetic process with a rate $\sim$5 s^{-1} both for the interaction of native cyt *c* and acid-unfolded state (data not shown), which correlates with the first fluorescence phase observed during unfolding and refolding of cyt *c* with L-PG micelles (k_1; Tables 1, 2). Thus, it appears that k_1 is probably associated with a heme deligation step preceding the main structural unfolding (k_2) in both the interaction of native and acid-unfolded cyt *c* with L-PG micelles. In the micelle-induced refolding, k_1 is probably associated with the displacement of nonnative His33 ligation to the heme iron known to be present in the unfolded state and to persist throughout the early phases of folding of cyt *c* in solution at neutral pH (Colón et al., 1996, 1997).

The main kinetic event (k_2) observed in unfolding (Table 2) and refolding (Table 1) is likely to correspond to the disruption of the hydrophobic core of the compact states N_s and $C_{w/s}$, respectively. These are represented by the kinetic steps $N_s \rightarrow D_i$ (Equation 1) and $C_{w/s} \rightarrow I_i$ (Equation 2) for the micelle-induced unfolding and refolding of cyt *c*, respectively. Both events carry the largest change in fluorescence (a_2; Tables 1, 2). However, a_2 tends to be larger for unfolding (up to 97%; Table 2) than for refolding (up to 80%; Table 1), with k_2 being slower for unfolding ($\sim$0.1 s^{-1}; Table 2) than for the refolding reaction ($\sim$0.6 s^{-1}; Table 1). These observations may indicate structural differences between N_s and $C_{w/s}$. N_s is expected to have a more tightly packed hydrophobic core than $C_{w/s}$ and thus likely to unfold slower. If N_s is more compact than $C_{w/s}$, it is also expected that the transition $N_s \rightarrow D_i$ would give rise to a larger Trp fluorescence change than $C_{w/s} \rightarrow I_i$.

In conclusion, the interaction of both native and acid-unfolded state of cyt *c* with L-PG micelles results in a common micelle-associated helical state H_L. Based on the equilibrium spectroscopic data, H_L has a native-like α-helix content (Fig. 3A), but it is a highly expanded state without a tightly packed hydrophobic core as revealed by (1) Trp59 fluorescence (Fig. 2), which shows a much larger Trp59-heme distance than in the native state; (2) perturbed heme ligation (Fig. 1) and heme environment (Fig. 3C); and (3) lack of specific native interactions involving Trp59 (Fig. 3B). Formation of H_L from the native state of cyt *c* requires the disruption of the tightly packed native hydrophobic core of cyt *c* ($N_s \rightarrow D_i$, Equation 1) prior to insertion into the lipid phase. This micelle-induced unfolding of cyt *c* occurs at a rate $\sim$0.1 s^{-1}, which is remarkably faster than the expected rate of unfolding in solution. Refolding of acid-unfolded cyt *c* with L-PG micelles involves an early highly helical collapsed state formed during the burst phase ($<$3 ms), and the observed main kinetic event reports on the opening of this early compact intermediate ($C_{w/s} \rightarrow I_i$, Equation 2) prior to insertion into the lipid micelle.

Biological implications

The study by Cortese et al. (1998) showed that, under physiological conditions, cyt *c* is found to be in equilibrium between the soluble state and conformations bound to the inner mitochondrial membrane. The authors suggested that the initial interaction with the membrane results in a surface associated state where cyt *c* retains a native-like secondary structure with an intrinsic electron transfer activity similar to that of the native soluble protein. A more deeply inserted state into the membrane was also identified and was associated with a reduced α-helix content and increased β-sheet structure under physiological ionic strength. This membrane-inserted form has a reduced electron transfer activity than native cyt *c* in solution or membrane-associated states at low ionic strength. Our current and previous studies (Pinheiro et al., 1997), and those by de Kruijff and coworkers (Jordi et al., 1989; de Jongh & de Kruijff, 1990), and Muga et al. (1991) have not detected significant changes in the secondary structure of cyt *c* upon binding to lipid membranes under low ionic strength. However, our studies bring further structural insight into the more native-like membrane-bound states of cyt *c* associated with high electron transfer activity reported by Cortese et al. (1998). Our findings suggest that the active state of cyt *c* associated with membranes is likely to have a disrupted Met80-heme ligation, expanded Trp59-heme distance, disrupted packing of core side chains and heme crevice, but retains a native-like α-helical structure.

A membrane-bound form of cyt *c* appears to be relevant to its role in apoptotic cell death (Jemmerson et al., 1999). This study showed that, in apoptotic and necrotic T hybridoma cells, a monoclonal antibody binds to a region of cyt *c* around amino acid residue 44, which is located close to the exposed heme crevice. The antibody did not recognise purified native cyt *c* or cyt *c* in permeabilized live cells, but recognized cyt *c* bound to phospholipid vesicles known to induce structural destabilization of native cyt *c*. Thus, the authors suggested that a membrane-bound conformationally altered form of cyt *c* might be the relevant form in caspase activation. Our studies support the interpretation that a membrane-triggered opening of the structure of cyt *c* could expose the domain required for antibody recognition. However, it remains

intriguing how a membrane-induced conformational state of the same protein could be involved in electron transfer activity in live cells and have a more sinister role, if released from mitochondria, during apoptotic cell death.

Materials and methods

Materials

Horse heart cyt *c* (type VI) was purchased from Sigma Chemical Co. (St. Louis, Missouri) and used without further purification. L-PG was acquired from Avanti Polar Lipids, Inc. (Birmingham, Alabama).

Sample preparation

Aqueous solutions of native cyt *c* were prepared in 10 mM potassium phosphate buffer at pH 7.0 (phosphate buffer). Protein concentrations were determined spectrophotometrically using a molar extinction coefficient of 2.95×10^4 M^{-1} cm^{-1} at 550 nm and pH 7.0 for the protein reduced with sodium dithionite (Margoliash & Walasek, 1967).

Acid-unfolded cyt *c* was prepared by diluting a concentrated H_2O solution of cyt *c* into 10 mM HCl, pH 2.0 (HCl solution). To remove any salt contaminants, which prevent the formation of the unfolded state of cyt *c*, the solution was passed through a fine grade Sephadex G-25 spin column pre-equilibrated with HCl solution.

L-PG micelles were prepared by hydration of the required amounts of lipid with phosphate buffer to produce a stock solution of micelles with an L-PG concentration of 20 mM. The buffer was deoxygenated with nitrogen gas prior to lipid hydration and the lipid suspension was sonicated for 30 min in a water bath sonicator (Ultrawave U-400) to ensure a homogeneous micelle size.

Absorbance measurements

Absorbance spectra in the Soret region (350–490 nm) were obtained for samples containing 10 μM cyt *c* in phosphate buffer and HCl solution, in the absence and presence of L-PG micelles, for lipid concentrations ranging from 1 to 10 mM. All spectra were measured against the appropriate reference (buffer for protein solutions or micelles for lipid/protein samples). Spectra were recorded at room temperature (~20 °C) on a JASCO V-550 UV/Vis spectrophotometer using cells of 5 mm pathlength.

Equilibrium fluorescence

Fluorescence spectra were obtained for samples containing 10 μM cyt *c* in phosphate buffer and HCl solution with and without lipid. Lipid concentrations were varied from 1 to 10 mM. The excitation wavelength was 295 nm (4 nm bandpass), and emission spectra were recorded from 300 to 450 nm (4 nm bandpass). All spectra were measured at room temperature (~20 °C) on a Perkin-Elmer LS50 spectrometer. Each spectrum was an average of eight scans. Spectra were corrected for backgrounds recorded for corresponding samples without protein (buffer for spectra of protein solutions or lipid micelles for spectra of lipid-protein samples).

Circular dichroism

CD spectra of far-UV (185–260 nm), near-UV (255–330 nm), as well as the Soret region (350–490 nm) were recorded on a JASCO J-715 spectropolarimeter. Spectra were obtained for samples containing 10 to 20 μM cyt *c* in phosphate buffer and HCl solution, in the absence and presence of varying concentrations of L-PG from 1 to 10 mM. CD spectra of the far-UV region were measured using quartz cells of 1 mm pathlength; for near-UV and Soret regions 5 mm pathlength cells were used. All spectra were corrected for their corresponding backgrounds. The measurements were recorded with a bandwidth of 1.0 nm and a scanning rate of 100 nm/min. Spectral resolution was 0.5 nm/min, and 4 (Soret) or 8 (far-UV and near-UV) scans were averaged per spectrum. The cell holder was thermostated with a circulating water bath, and all spectra were recorded at 20 ± 0.2 °C.

Stopped-flow fluorescence kinetics

Kinetic fluorescence measurements were performed on a Micro Volume Stopped-Flow Reaction Analyser SX.18MV (Applied Photophysics Ltd., Leatherhead, UK), equipped with a modified T mixer designed by Applied Photophysics, and a $2 \times 1 \times 10$ mm flow cell. A 150 W xenon arc lamp (OSRAM, Germany) and monochromator were used for excitation at 295 nm (4.2 nm bandwidth) along the 10 mm axis of the cell. The fluorescence emission was measured in the 2 mm direction, using a high pass filter with a 320 nm cut-off and an electronic filter with a time constant of 100 μs. All kinetic experiments were performed at 20 ± 0.2 °C. Micelle-induced unfolding of cyt *c* was initiated by mixing five parts of L-PG micelles in phosphate buffer with one part of cyt *c* in phosphate buffer (5:1, v/v). Refolding of cyt *c* driven by lipid micelles was initiated by 5:1 (v/v) mixing of L-PG micelles in phosphate buffer with acid-unfolded cyt *c* in HCl solution (5 parts of lipid to 1 part of protein). The final pH of mixtures of acid-unfolding cyt *c* with lipid micelles was 6.8. Final protein concentration varied from 4 to 20 μM and lipid from 1 to 10 mM. The changes in fluorescence emission were monitored over a timescale up to 100 s. The dead time of the stopped-flow instrument operating in 5:1 mixing was 2.5–3.0 ms. One thousand data points were acquired in a logarithmic time base. An average of four kinetic traces was taken per sample. Data acquisition and analysis were carried out using the Applied Photophysics software. The kinetic parameters were obtained by nonlinear least-squares analysis using a minimum number of exponential phases. Kinetic traces were corrected for lipid scattering background (typically a deviation from buffer of no more than 1% of the fluorescence intensity of the unfolded state) and normalized to the fluorescence level of the acid-unfolded state.

Acknowledgments

This work has been supported by the Royal Society and the Biotechnology and Biological Science Research Council (BBSRC) (Grant 88/B09547; and a PhD studentship to NS). TJTP is a Royal Society University Research Fellow. We also thank Dr. S.K. Kulkarni for her critical reading of the manuscript.

References

Babul J, Stellwagen E. 1972. Participation of the protein ligands in the folding of cytochrome *c*. *Biochemistry 11*:1195–1200.

Bryson EA, Rankin SE, Carey M, Watts A, Pinheiro TJT. 1999. Folding of apocytochrome *c* in lipid micelles: Formation of α-helix precedes membrane insertion. *Biochemistry 38*:9758–9767.

Bushnell GW, Louie GV, Brayer GD. 1990. High-resolution three-dimensional structure of horse cytochrome *c*. *J Mol Biol 214*:585–595.

Bychkova VE, Ptitsyn OB. 1993. The molten globule in vitro and in vivo. *Chemtracts Biochem Mol Biol 4*:133–163.

Chan C-K, Takahashi S, Rousseau DL, Eaton WA, Hofrichter J. 1997. Submillisecond protein folding kinetics studied by ultrarapid mixing. *Proc Natl Acad Sci USA 94*:1779–1784.

Colón W, Elöve GA, Wakem LP, Sherman F, Roder H. 1996. Side chain packing of the N- and C-terminal helices plays a critical role in the kinetics of cytochrome *c* folding. *Biochemistry 35*:5538–5549.

Colón W, Elöve GA, Wakem LP, Sherman F, Roder H. 1997. Identification of the predominant non-native histidine ligand in unfolded cytochrome *c*. *Biochemistry 36*:12535–12541.

Cortese JD, Voglino AL, Hackenbrock CR. 1998. Multiple conformations of physiological membrane-bound cytochrome *c*. *Biochemistry 37*:6402–6409.

Davies AM, Guillemette JG, Smith M, Greenwood C, Thurgood AGP, Mauk AG, Moore GR. 1993. Redesign of the interior of mitochondrial cytochrome *c* by site-directed mutagenesis. *Biochemistry 32*:5431–5435.

de Jongh HHJ, de Kruijff B. 1990. The conformational changes of apocytochrome *c* upon binding to phospholipid vesicles and micelles of phospholipid based detergents. A circular dichroism study. *Biochim Biophys Acta 1029*:105–112.

de Jongh HHJ, Killian JA, de Kruijff B. 1992. A water lipid interface induces a highly dynamic folded state in apocytochrome *c* and which may represent a common folding intermediate. *Biochemistry 31*:1636–1643.

Elöve GA, Bhuyan AK, Roder H. 1994. Kinetic mechanism of cytochrome *c* folding: Involvement of the heme and its ligands. *Biochemistry 33*:6925–6934.

Elöve GA, Chaffotte AF, Roder H, Goldberg ME. 1992. Early steps in cytochrome *c* folding probed by time-resolved circular dichroism and fluorescence spectroscopy. *Biochemistry 31*:6876–6883.

Gierasch LM. 1989. Signal sequences. *Biochemistry 28*:923–930.

Gupte SS, Hackenbrock CR. 1988. The role of cytochrome *c* diffusion in mitochondrial electron transport. *J Biol Chem 263*:5248–5253.

Hildebrandt P, Heimburg T, Marsh D, Powell GL. 1990. Conformational changes in cytochrome *c* and cytochrome *c* oxidase upon complex formation: A resonance Raman study. *Biochemistry 29*:1661–1668.

Hu YM, Benedict MA, Ding LY, Munez G. 1999. Role of cytochrome *c* and dATP/ATP hydrolysis in Apaf-1-mediated caspase-9 activation and apoptosis. *EMBO J 18*:3586–3595.

Jemmerson R, Liu J, Hausauer D, Lam K-P, Mondino A, Nelson RD. 1999. A conformational change in cytochrome *c* of apoptotic and necrotic cells is detected by monoclonal antibody binding and mimicked by association of native antigen with synthetic vesicles. *Biochemistry 38*:3599–3609.

Jordi W, Li-Xin Z, Pilon M, Demel RA, de Kruijff B. 1989. The importance of the amino terminus of the mitochondrial precursor protein apocytochrome *c* for translocation across model membranes. *J Biol Chem 264*:2292–2301.

Liu X, Kim CN, Yang J, Jemmerson R, Wang X. 1996. Induction of apoptotic program in cell-free extracts: Requirement for dATP and cytochrome *c*. *Cell 86*:147–157.

Maloy WL, Kari UP. 1995. Structure-activity studies on magainins and other host defence peptides. *Biopolymers 37*:105–122.

Margoliash E, Walasek OF. 1967. Cytochrome *c* from vertebrate and invertebrate sources. *Methods Enzymol 10*:339–348.

Muga A, Mantsch HH, Surewicz WK. 1991. Membrane binding induces destabilization of cytochrome *c* structure. *Biochemistry 30*:7219–7224.

Myer YP. 1968. Conformations of cytochromes. III. Effect of urea, temperature, extrinsic ligands, and pH variation on the conformation of horse heart ferricytochrome *c*. *Biochemistry 7*:765–776.

Pinheiro TJT. 1994. The interaction of horse heart cytochrome *c* with phospholipid bilayers. Structural and dynamic effects. *Biochimie 76*:489–500.

Pinheiro TJT, Elöve GA, Watts A, Roder H. 1997. Structural and kinetic description of cytochrome *c* unfolding induced by the interaction with lipid vesicles. *Biochemistry 36*:13122–13132.

Pinheiro TJT, Watts A. 1994. Lipid specificity in the interaction of cytochrome *c* with anionic phospholipid membranes. *Biochemistry 33*:2451–2458.

Prats M, Teissié J, Toccane JF. 1986. Lateral proton conduction at lipid-water interfaces and its implications for the chemiosmotic-coupling hypothesis. *Nature 322*:756–758.

Ptitsyn OB. 1995. Molten globule and protein folding. *Adv Protein Chem 47*:83–229.

Rankin SE, Watts A, Pinheiro TJT. 1998. Electrostatic and hydrophobic contributions to the folding mechanism of apocytochrome *c* driven by the interaction with lipid. *Biochemistry 37*:12588–12595.

Rankin SE, Watts A, Roder H, Pinheiro TJT. 1999. Folding of apocytochrome *c* induced by the interaction with negatively charged lipid micelles proceeds via a collapsed intermediate state. *Protein Sci 8*:381–393.

Roder H, Elöve GA, Englander SW. 1988. Structural characterisation of folding intermediates in cytochrome *c* by H-exchange labelling and proton NMR. *Nature 335*:700–704.

Sauder JM, MacKenzie NE, Roder H. 1996. Kinetic mechanism of folding and unfolding of *Rhodobacter capsulatus* cytochrome c_2. *Biochemistry 35*:16852–16862.

Shai Y. 1994. Pardaxin: Channel formation by a shark repellent peptide from fish. *Toxicology 87*:109–129.

Shastry MCR, Roder H. 1998. Evidence for barrier-limited protein folding kinetics on the microsecond time scale. *Nat Struct Biol 5*:385–392.

Sosnick TR, Mayne L, Englander SW. 1996. Molecular collapse: The rate-limiting step in two-state cytochrome *c* folding. *Proteins Struct Funct Genet 24*:413–426.

Speck SH, Neu CA, Swanson MS, Margoliash E. 1983. Role of phospholipid in the low affinity reaction between cytochrome *c* and cytochrome oxidase. *FEBS Lett 164*:379–382.

Spooner PJR, Watts A. 1991. Reversible unfolding of cytochrome *c* upon interaction with cardiolipin bilayers. 1. Evidence from deuterium NMR measurements. *Biochemistry 30*:3871–3879.

Thiaudière E, Siffert O, Talbot J-C, Bolard J, Alouf JE, Dufourcq J. 1991. The amphiphilic α-helix concept. Consequences on the structure of staphylococcal δ-toxin in solution and bound to lipids. *Eur J Biochem 195*:203–213.

Tsong TY. 1974. The Trp-59 fluorescence of ferricytochrome *c* as a sensitive measure of the overall protein conformation. *J Mol Biol 249*:1988–1990.

van der Goot FG, González-Mañas JM, Lakey JH, Pattus F. 1991. A "molten-globule" membrane-insertion intermediate of the pore-forming domain of colicin A. *Nature 354*:408–410.

Vécsey-Semjén B, Lesieur C, Möllby R, van der Goot FG. 1997. Conformational changes due to membrane binding and channel formation by staphylococcal α-toxin. *J Biol Chem 272*:5709–5717.

Vik SB, Georgevich G, Capaldi RA. 1981. Diphosphadidylcholine is required for optimal activity of beef heart cytochrome *c* oxidase. *Proc Natl Acad Sci USA 78*:1456–1460.

Zakharov SD, Lindeberg M, Griko Y, Salamon Z, Tollin G, Prendergast FG, Cramer WA. 1998. Membrane-bound state of the colicin E1 channel domain as an extended two-dimensional helical array. *Proc Natl Acad Sci USA 95*:4282–4287.